Chapter 6: Experimental investigations of SPNCL using mono/hybrid nano-oils

This chapter presents the experimental investigation for the performance assessment of VHHC configuration of SPNCL in the medium temperature range (100^{o}-250^{o}). This temperature range is relevant for various applications, such as manufacturing soaps and synthetic rubber, process heating, solar heating and cooking. Suitable working fluids, viz. thermal oil (Therminol VP1) and vegetable oil (Soyabean), having a high volumetric expansion coefficient, high thermal conductivity, commercial/local availability and low cost, are selected for experimentations. Nano-oils are prepared by dispersing nanoparticles in Therminol VP1 and Soyabean oils (base fluid) for the reported experiments. The details of the experimental setup, parametric investigations and the corresponding measurements are presented subsequently. In this chapter, the terminologies primary or working fluids, and secondary fluid or coolant, are used interchangeably.

6.1 Experimentation methodology

6.1.1 Experimental setup and procedure

The photographic view of the installed SPNCL experimental facility is presented in Fig.6.1. Geometrically, the loop is identical to the presented setup in Chapter 5, except (a) the electromagnetic flow meter is replaced by a borosilicate glass tube, which helps to visualize the flow, and (b) U tube manometer is connected at the lower horizontal leg of length 0.7 m to measure pressure drop. Water with dissolved (very small amount) Potassium permanganate ($KMnO_4$) has been used as the manometric fluid. The presence of the $KMnO_4$ turns the water into a pink color liquid and helps in a clear visual of the oil and water interface. The experiments were performed using different nano-oils with Therminol

VP1 and Soyabean oil as the base fluids. Here, the effect of different power inputs and loop inclination (clockwise and counter-clockwise) have been investigated. The same procedure has been followed as discussed in Chapter 5 section 5.2.2.

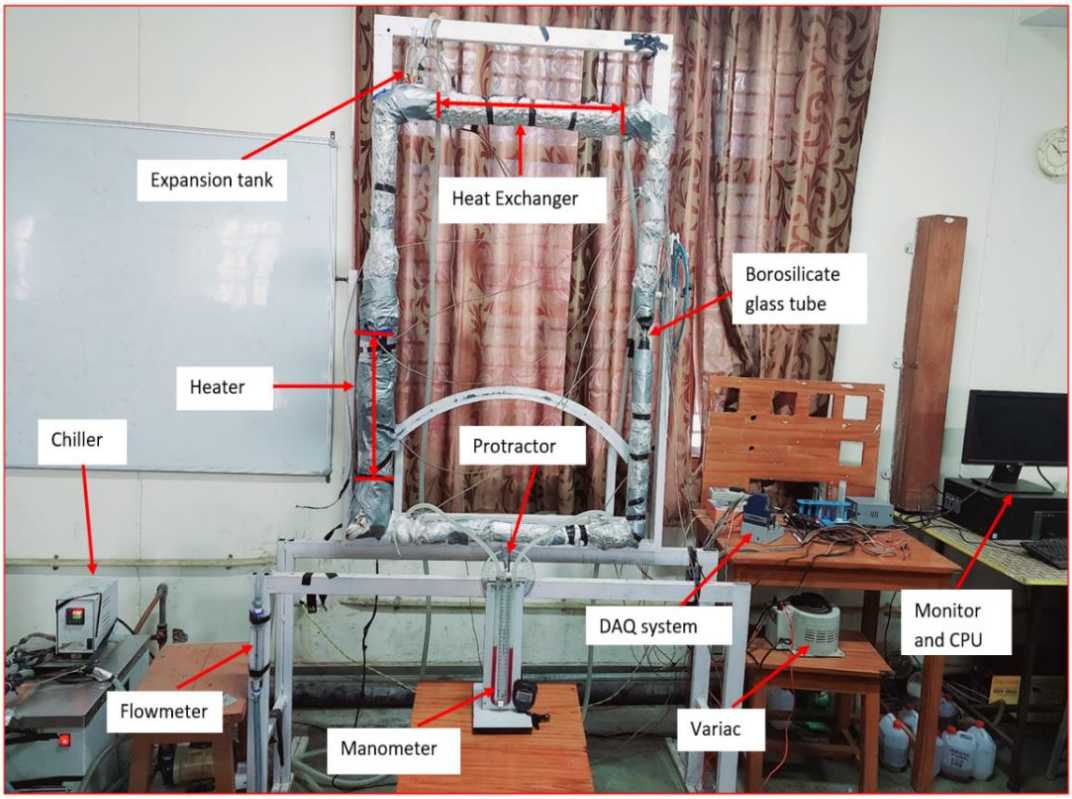

Fig. 6.1 Photographic view of the installed single-phase natural circulation loop (SPNCL) experimental facility.

6.1.2 Nano-oil preparation, characterization and properties

The considered nano-oils have been prepared and characterized similarly to water-based nanofluids, as discussed in chapter 5. The temperature-dependent thermophysical properties of Therminol VP1 have been taken from the EES library [111]. For Soyabean oil, these have been calculated from the following equations [120]:

Density (kg/m^3):

$$\rho = 1039.225 - 0.397T \tag{6.1}$$

Specific Heat (J/kg-K)

$$c_p = 1024 + 3T \tag{6.2}$$

Thermal conductivity (W/m-K):

$$k = 0.134 + 0.0001T \tag{6.3}$$

Dynamic Viscosity (N-s/m^2):

$$\ln(\mu \times 10^3) = \frac{0.7442T}{-240.4647+T} \tag{6.4}$$

where the Temperature T is in K. The thermophysical properties of the oil and oil-based mono/hybrid nanofluids have been calculated by using models and correlations, as discussed in chapter 3. The variations of thermophysical properties with temperature for Therminol VP1 and Soyabean oil are shown in Fig. 6.2.

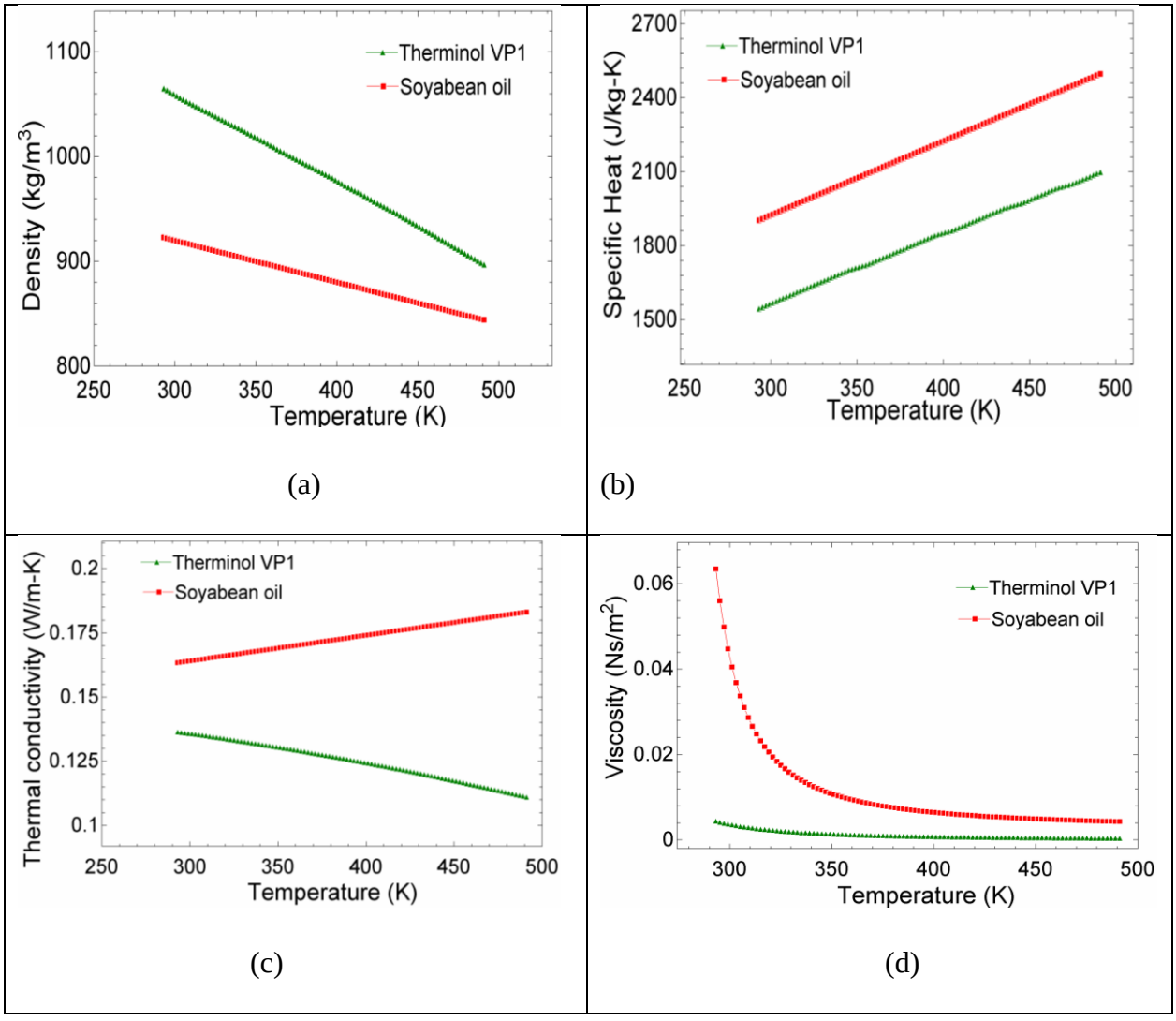

Fig. 6.2 Variation of thermophysical properties: (a) density, (b) specific heat capacity, (c) thermal conductivity, and (d) absolute viscosity for the primary fluids

6.1.3 Evaluation of performance parameters

To compare the various working fluids, three crucial performance parameters are used: the buoyancy force-induced mass flow rate, heat exchanger effectiveness, and the total entropy generation rate. This provides the energy-exergy performance of the SPNCL system. These performance parameters are calculated by;

a). Buoyancy force-induced mass flow rate (MFR): It predicts the heat transport ability of the SPNCL system obtained using the following energy balance:

$$\dot{m} = \frac{Q - h_a A_s (T_{H,ins} - T_a)}{c_p (T_{H,out} - T_{H,in})}, \tag{6.5}$$

where Q, A_s, h_a, T_s, $T_{H,ins}$, Ta, $T_{H,in}$, and $T_{H,out}$ is the power input supplied, external surface area of the heater, ambient heat transfer coefficient, average external surface temperature of the insulated heating section, ambient temperature, inlet and outlet temperature of the primary fluid in the heater respectively. The average external surface temperature for the insulated heater is defined as the arithmetic mean of the measured values using the three equally-spaced thermocouples. The heat transfer coefficient (h_a) for the air side (ambient) is estimated using the following Nusselt number correlation by Churchill and Chu [117]:

$$Nu_a = \frac{h_a L}{k_a} = \{0.68 + \frac{0.670 Ra_L^{1/4}}{[1 + (0.492 \Pr_a)^{9/16}]^{4/9}}\}, \text{ for Ra} < 10^9 \tag{6.6}$$

$$Nu_a = \frac{h_a L}{k_a} = \{0.825 + \frac{0.387 Ra_L^{1/6}}{[1 + (0.492 \Pr_a)^{9/16}]^{8/27}}\}, \text{ for Ra} > 10^9 \tag{6.7}$$

b). Heat exchanger effectiveness (HEE): It predicts the heat transfer capability of the system as given by [52],

$$\varepsilon = \frac{T_{C,in} - T_{C,out}}{T_{C,in} - T_{S,in}} \tag{6.8}$$

Where, $T_{C,out}$ *and* $T_{C,in}$ are the outlet and inlet temperature of the loop fluid in the heat exchanger, and $T_{S,in}$ is the secondary fluid inlet temperature.

c. *Total entropy generation rate (TEGR)*: It predicts the exergetic performance of the loop. For heating, cooling, hot and cold leg segments, the TEGR is derived from entropy generation principle and given respectively,

$$S_{gen,H} = \dot{m}\left[c_{p,H} \ln\left(\frac{T_{H,out}}{T_{H,in}}\right) + \frac{f_H L_H \dot{m}^2}{2d\rho_H^2 A^2 T_H} - \frac{c_{p,H}\left(T_{H,out} - T_{H,in}\right)}{T_{wall,H}} \right] \tag{6.9}$$

$$S_{gen,C} = \dot{m}\left[c_p \ln\left(\frac{T_{C,out}}{T_{C,in}}\right) + \frac{fL_C \dot{m}^2}{2d\rho_{C,avg}^2 A^2 T_{C,avg}} \right] + m_S c_{p,S} \ln\left(\frac{T_{S,out}}{T_{S,in}}\right) \tag{6.10}$$

$$S_{gen,leg} = \frac{\dot{m}^3}{2dA^2}\left[\frac{f_h L_h}{\rho_h^2 T_h} + \frac{f_c L_c}{\rho_c^2 T_c} \right] \tag{6.11}$$

Consequently, the TEGR is present by,

$$S_{gen,t} = S_{gen,H} + S_{gen,C} + S_{gen,leg} \tag{6.12}$$

Where the primary fluid inlet and outlet temperatures in the heater and heat exchanger, respectively, are denoted by $T_{H,in}$, $T_{H,out}$, $T_{C,in}$ and $T_{C,out}$.

T_H, T_C, T_h and T_c are the mean of inlet and outlet temperature of the loop fluid in the heater, Heat exchanger, hot, and cold leg, respectively.

f_H, f_C, f_h and f_c are the friction factor calculated in the Heating, Heat exchanger, Hot leg, and Cold leg sections respectively. The friction factor used, which is suitable for the SPNCL system, is given by [10].

6.1.4 Uncertainty analysis

The maximum uncertainties of the calculated parameters for TVP1 and Soyabean oil are listed in Table 6.1 and Table 6.2, respectively.

Table 6.1 Maximum uncertainties of the calculated parameters for the TVP1.

Parameters	**Uncertainty value (%)**
Mass flow rate, $\dot{m}$ (kg/s)	±2.2
Effectiveness, ε	±4.5
Total entropy generation rate, $S_{gen,t}$ (W/K)	±1.6

Table 6.2 Maximum uncertainties of the calculated parameters for the Soyabean oil.

Parameters	**Uncertainty value (%)**
Mass flow rate, $\dot{m}$ (kg/s)	±1.2
Effectiveness, ε	±2.4
Total entropy generation rate, $S_{gen,t}$ (W/K)	±1.1

6.2 Results and discussion

This experimental campaign presents the effect of thermal oil (TVP1), Vegetable oil (Soyabean), nano-oils, input power, and loop inclination. In the present experimental analysis, our aim is to analyze the exegetic and energetic performance of the SPNCL loop using different oils and nano-oils for the constant heat flux condition and constant sink temperature condition (achieved by maintaining a high coolant flow rate). This boundary

condition is useful for the cooling application like cooling of an engine, where the heat sink is atmosphere, and decay heat removal in a nuclear reactor, where the heat sink is water pool.

The operating parameters are given in Table 6.3.

Table 6.3 Operating parameters for VHHC configuration of SPNCL.

Input Parameters	Values/Range
Power input	200, 400, 600, 800 W
Loop inclination	0^o, 30^o, 60^o
Coolant flow rate	5 LPM
Coolant inlet temperature	295 K
Coolant fluid	Water
Pressure inside loop	1 atm
Type of nanoparticles	Al_2O_3, CuO, SiC, CNT
Working fluids	Thermal oil: Therminol VP1, Al_2O_3+Therminol VP1, Al_2O_3+CuO+Therminol VP1, Al_2O_3+SiC+ Therminol VP1, Al_2O_3+CNT+ Therminol VP1 Vegetable oil: Soyabean, Al_2O_3+Soyabean, Al_2O_3+CuO+ Soyabean, Al_2O_3+SiC+ Soyabean, Al_2O_3+CNT+Soyabean
Nanoparticle volume concentration	$\phi = 0.1\%$

6.2.1 Repeatability test

The repeatability test has been performed to check the consistency of the experimental result. The measured soyabean oil temperature at the inlet and outlet of heater is reported in Fig. 6.3 for an input power of 400 W and coolant temperature of 295K, this reveals that

the deviation between the measured values is within 3%. Therefore, the repeatability is reassured for the designed loop and the performed experiments.

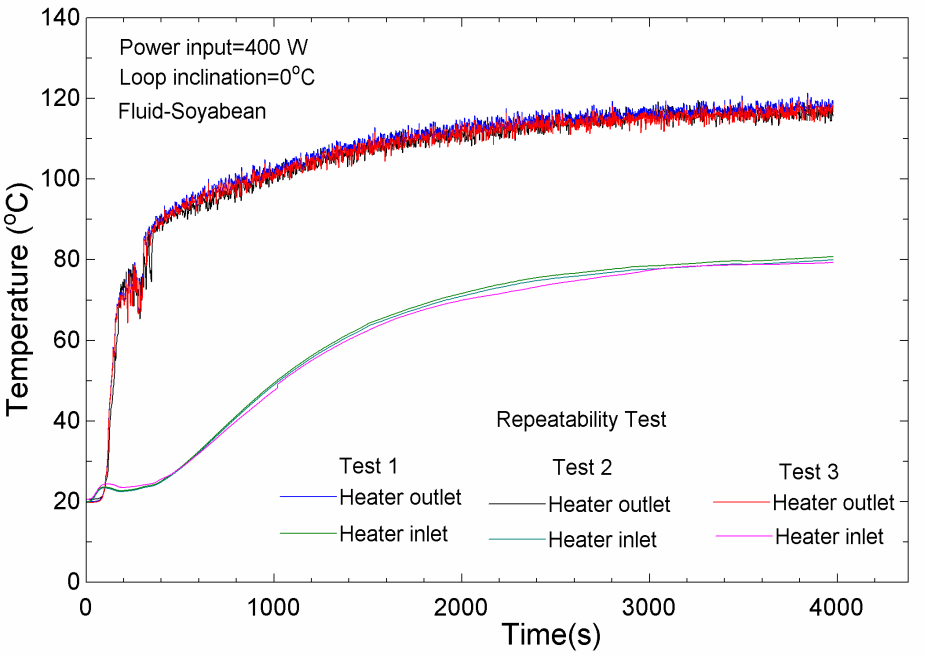

Fig. 6.3 The measured temperature with Soyabean oil at the inlet and outlet of heater for three different experiments and at an identical operating condition for repeatability.

6.2.2 Comparison of experimental and numerical results

The experimentally obtained temperature difference in TVP1 and Soyabean oil across the heater is compared with the most general numerically obtained values for an input power of 400 W, as shown in Fig. 6.4. The details of the developed numerical model (case vi) are discussed in Chapter 4. This comparison reveals (a) an over-prediction of temperature difference up to 20 % during the unsteady phase for TVP1 and a smaller relative deviation for Soyabean oil and (b) the steady-state condition is fairly well reproduced for TVP1 beyond 2500 seconds and for Soyabean oil beyond 900 seconds. The deviation in the early transient period may be due to the fully developed friction factor considered in the present numerical code. This reveals the capability and limitation of the developed numerical model and infers the possibility of further improvement.

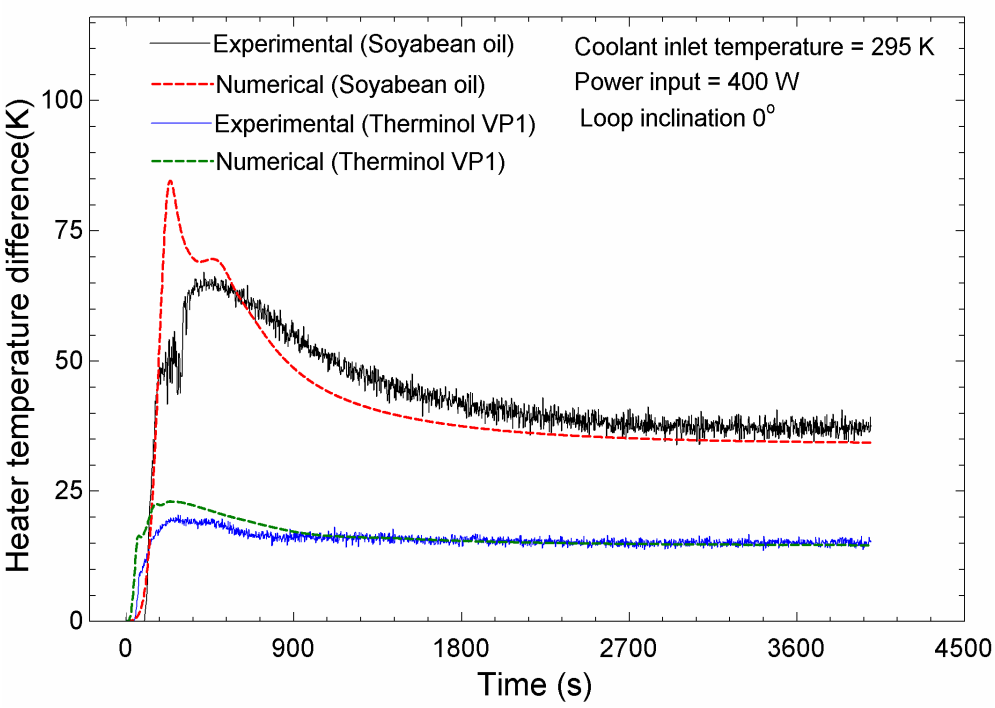

Fig. 6.4 A comparison between the experimental and numerical temperature difference across the heater for an input power of 400 W at the transient and steady-state conditions.

6.2.3 Transient behavior of SPNCL for mono/hybrid nano-oils

Figure 6.5 and Figure 6.6 show the experimentally obtained temperature difference across the heater for TVP1 and Soyabean oil-based mono/hybrid nanofluids at an input power of 400 W, respectively. All the working fluids show a similar trend, viz. initially, the heater temperature difference increases and attains a maximum peak, then starts decreasing with time and eventually attains a steady-state condition. The behavior is attributed to the initial disbalance between the buoyancy and friction force, which eventually stabilizes at a certain instant for TVP1 and Soyabean oil. This assessment shows Al_2O_3+CuO and Al_2O_3+SiC based nano-oil displays the highest and lowest values of temperature difference in comparison to other nano-oils. These may be attributed to the different mass flow rate arising from the thermophysical properties of these different nano-oils. Thus, it may be inferred that the nanoparticles may be carefully selected. Also, further investigation is recommended to obtain a better understanding.

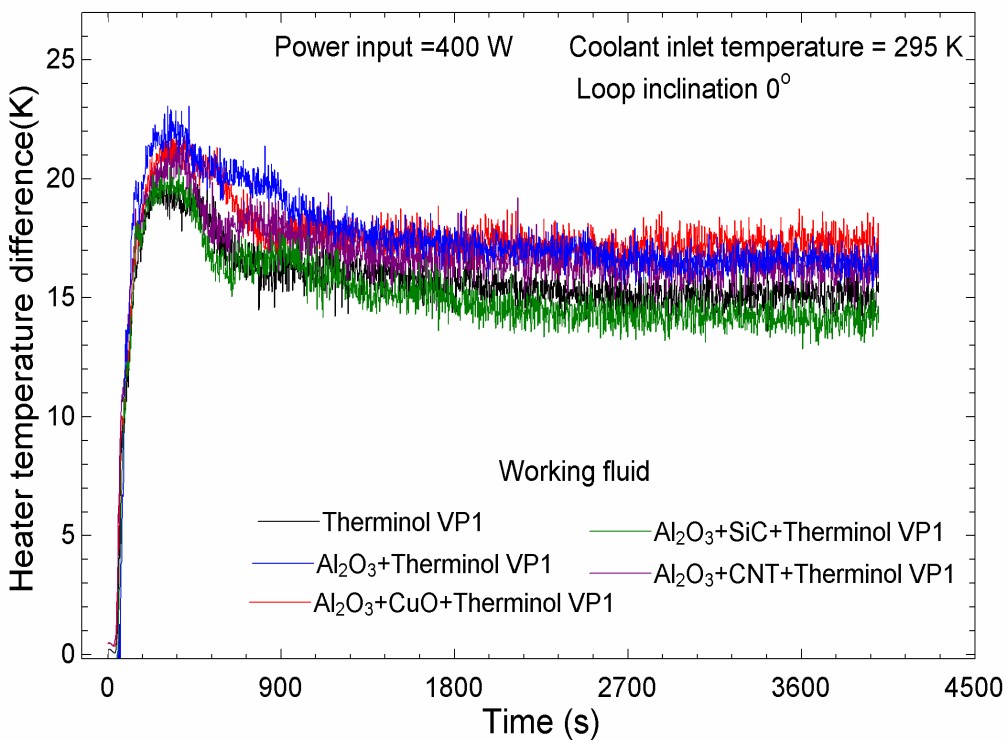

Fig. 6.5 Experimental temperature difference across the heater for the TVP1-based mono and hybrid nano-oils.

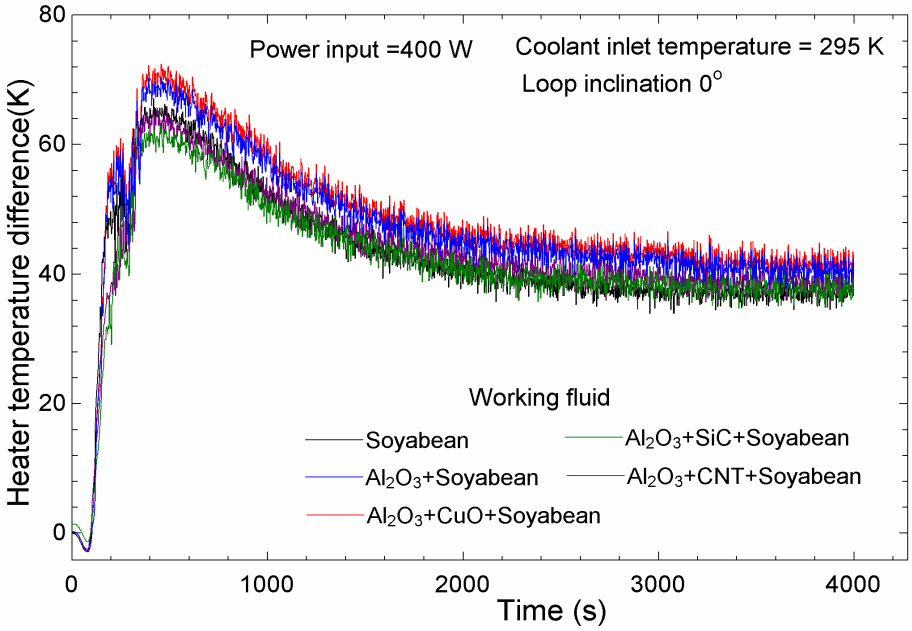

Fig. 6.6 Experimentally obtained temperature difference across the heater for the Soyabean oil-based mono and hybrid nano-oils.

6.2.4 Effect of input power on the transient and steady-state performance parameters

The transient and steady-state performance analyses for VHHC configuration of SPNCL, using TVP1 and Soyabean oil-based mono/hybrid nano-oils, at different input powers 200 W, 400 W, 600 W and 800 W, have been performed. Figure 6.7 and Figure 6.8 illustrate the evolution of temperature difference across the heater for TVP1 and Soyabean oil, respectively. These figures reveal distinctly different natures of the temperature difference for TVP1 and Soyabean oil with power input. Figure 6.6 shows that the temperature difference increases with the input powers, whereas Figure 6.7 shows that the temperature difference increases in the transient region; and decreases in the steady-state region. The reason behind this observation is that at higher power input, the loop average temperature increases; as a result, the soyabean oil viscosity decreases rapidly, reducing the frictional force, increasing the mass flow rate, and reducing the temperature difference. These figures also reveal that the time required to attain maximum temperature difference and to achieve steady-state decreases with the input power due to the early establishment of the flow, on account of a density difference between the hot leg and cold leg. The Therminol VP1 oil shows a quicker establishment of the flow and steady state than the soyabean oil, can be interpreted from the maximum peak attainment time.

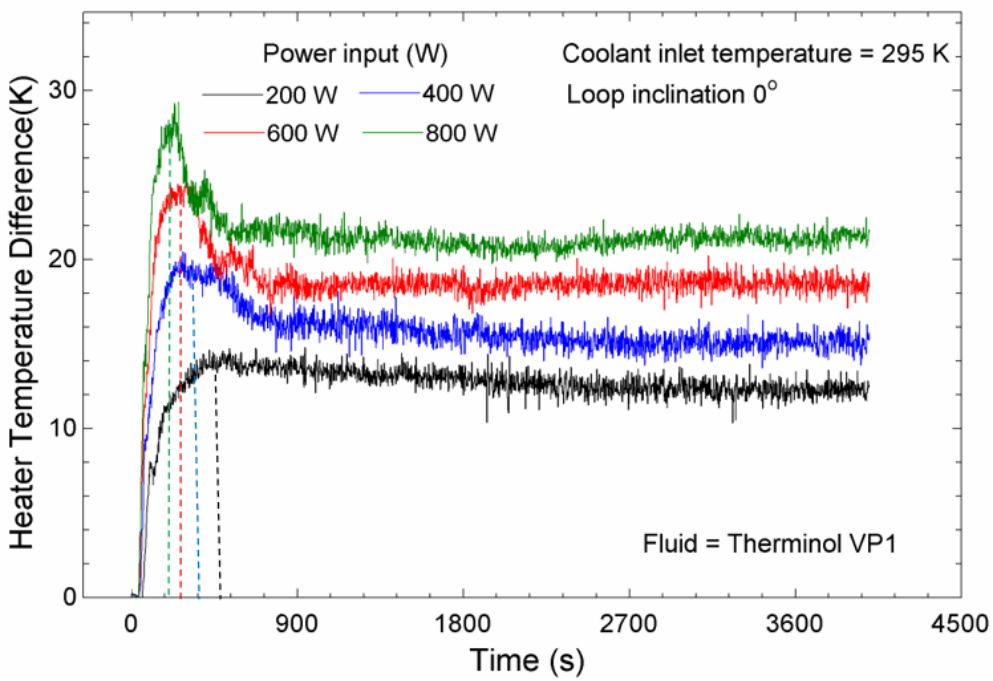

Fig. 6.7 Experimentally obtained temperature difference across the heater for TVP1 at different input powers

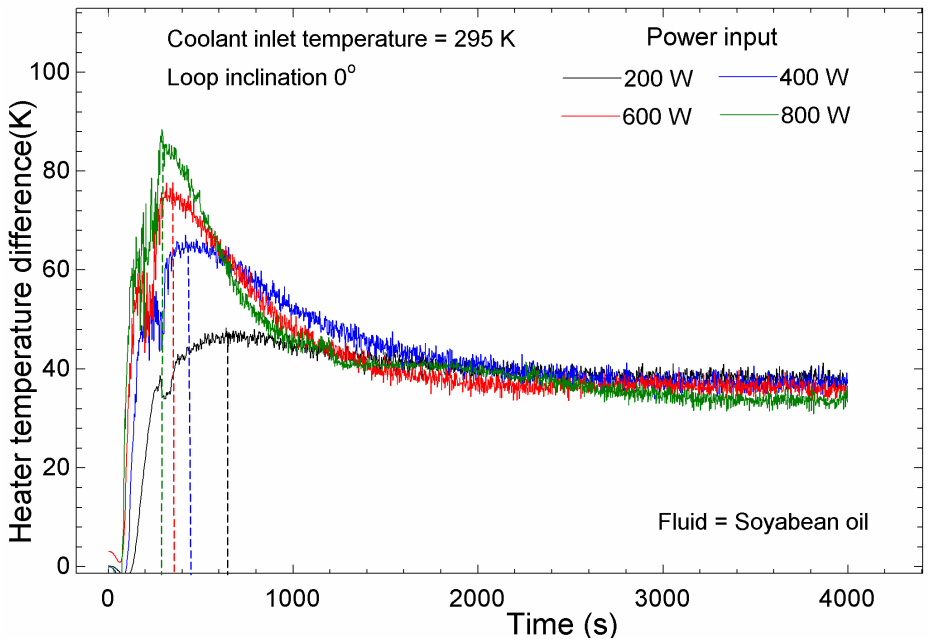

Fig. 6.8 Experimentally obtained temperature difference across the heater for Soyabean oil at different input powers.

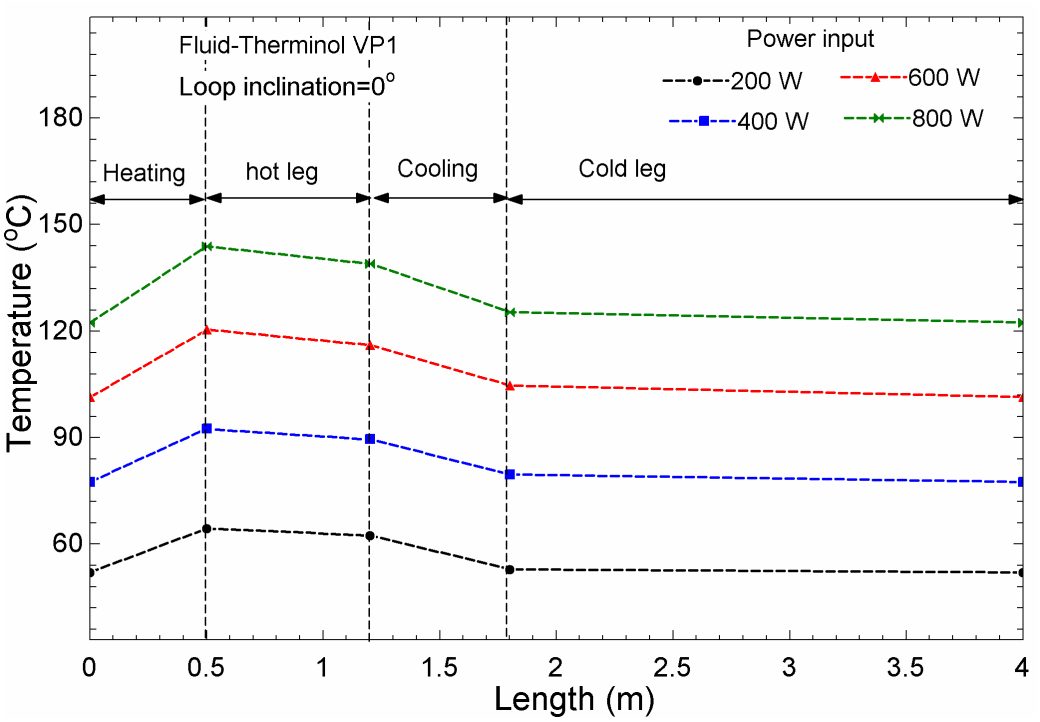

(a)

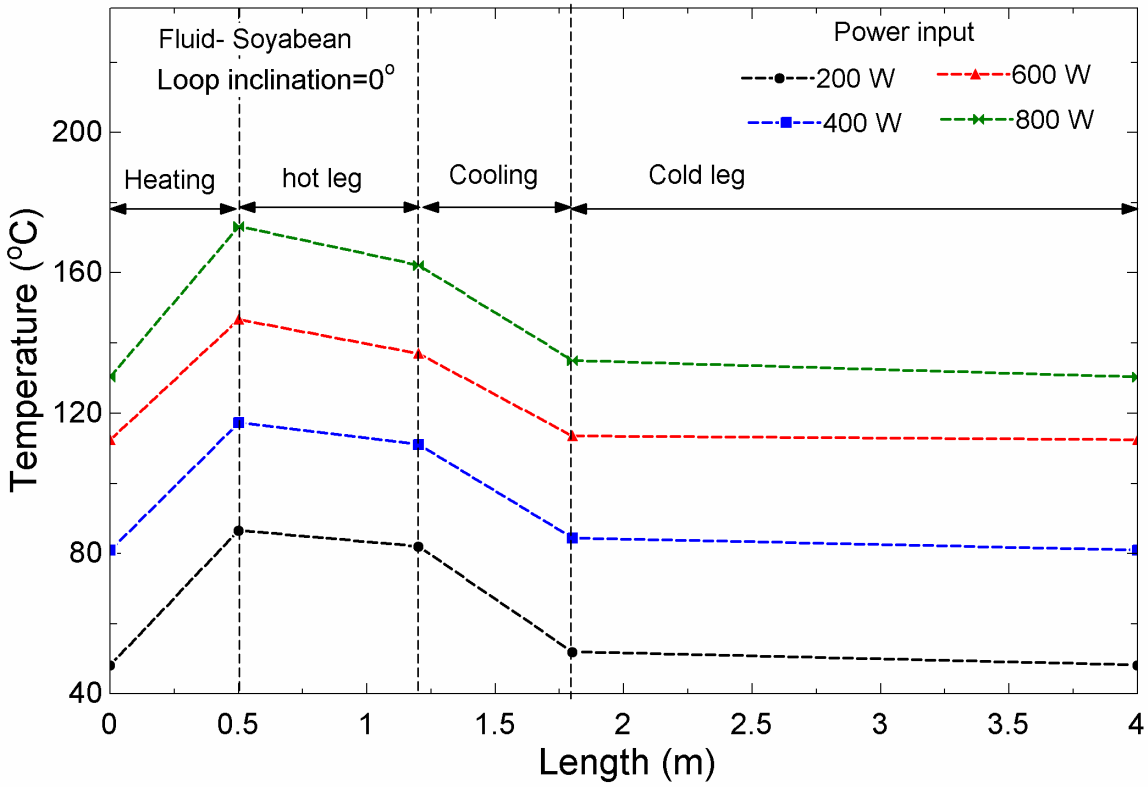

(b)

Fig. 6.9 Temperature distribution along loop length at different power input for (a) Therminol VP1 and (b) soyabean oil.

Fig.6.9 shows the temperature distribution along the loop length for different Therminol VP1and soyabean oil with Power input. The maximum temperature inside the loop is observed for the soyabean oil about 180 ^{O}C and 140 ^{O}C for Therminol VP1 at 800 W.

Fig. 6.10 and Fig.6.11 show the estimated steady-state mass flow rate for TVP1, Soyabean oil and their nano-oils for different input powers. The following may be inferred from these figures:

(a) Increasing mass flow rate with input power for a relatively higher buoyancy comparison to the friction force, arising out of the temperature difference between the hot leg and the cold leg.

(b) Decrease and then increase in the mass flow rates for TVP1 with spherical-shaped nanoparticles (Al_2O_3+TVP1, Al_2O_3+SiC+TVP1, and Al_2O_3+CuO+ TVP1), whereas reduction in mass flow rate is observed for TVP1 with cylindrical-shaped nanoparticles in comparison to that of the pure TVP1. The dominance of buoyancy enhances the mass flow rate, while the dominance of the viscous force reduces the mass flow rate;

(c) As the input power increases, the flow regime changes from laminar to turbulent at ~400 W (Re = 1200), since in SPNCL, the flow regime changes at a lower Reynolds number as reported in the literature. Therefore, the relative effect of frictional force decreases because of lower dominance of viscosity, and buoyant force starts dominating because of the suspended nanoparticles. This observation infers that the addition of nanoparticles at a high input power is more beneficial compared to low input power. The maximum Reynolds number for Therminol VP1-based mono/hybrid nanofluids is ~2550, corresponding to the highest power input.

(d) The reduction in mass flow rate is for all the soyabean-oil-based nano-oils in comparison to the pure oil. This is attributed to the laminar flow regime for the maximum Reynolds number ~200 at the highest input power 800 W.

(e) The mass flow rate is higher for the nano-oils with spherical-shaped nanoparticles (Al_2O_3+SiC, and Al_2O_3+CuO) in comparison to the cylindrical-shaped nanoparticle (Al_2O_3+MWCNT). These clearly show that the shape and properties of nanoparticle influences the mass flow rate. In general, a higher viscosity arising out of the shape-related wetted surface area leads to a lower mass flow rate, which is expected.

(f) The maximum increment in the mass flow rate is observed for Al_2O_3+Therminol VP1 (6.20%) and the maximum reduction in the mass flow rate is observed for Al_2O_3+MWCNT+ Therminol VP1 (5.9%) compared to Therminol VP1 at 800 W power input.

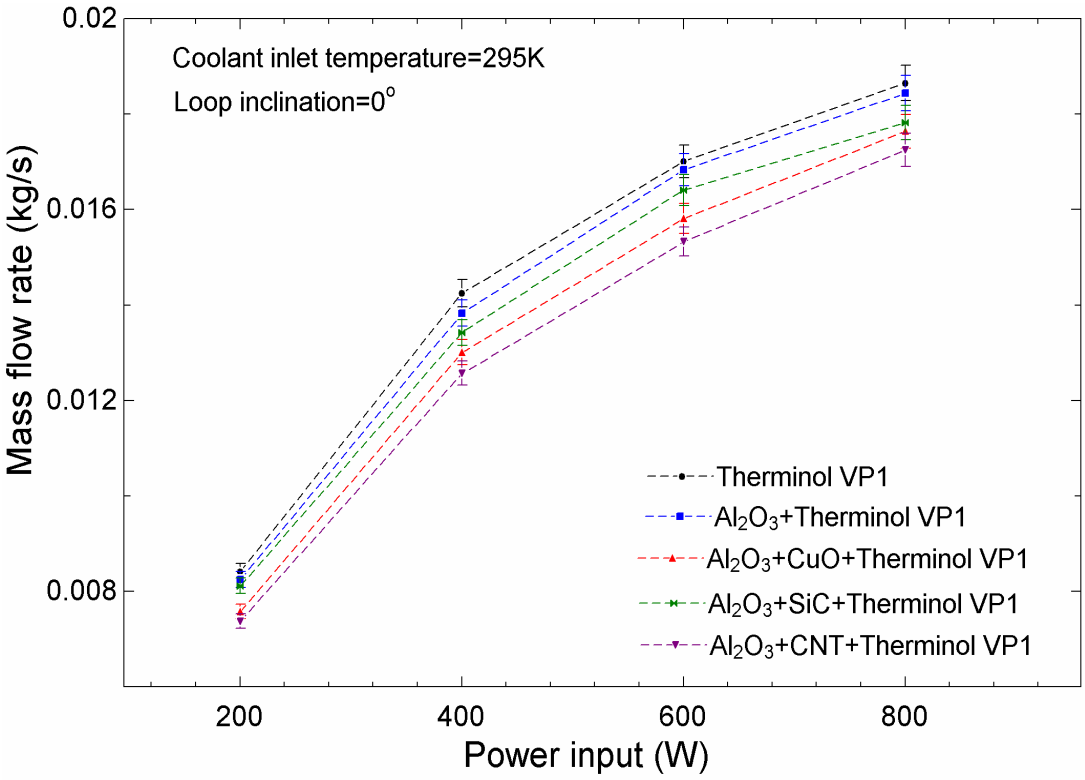

Fig. 6.10 Steady state mass flow rate for different Therminol VP1-based mono/hybrid nanofluids with power input.

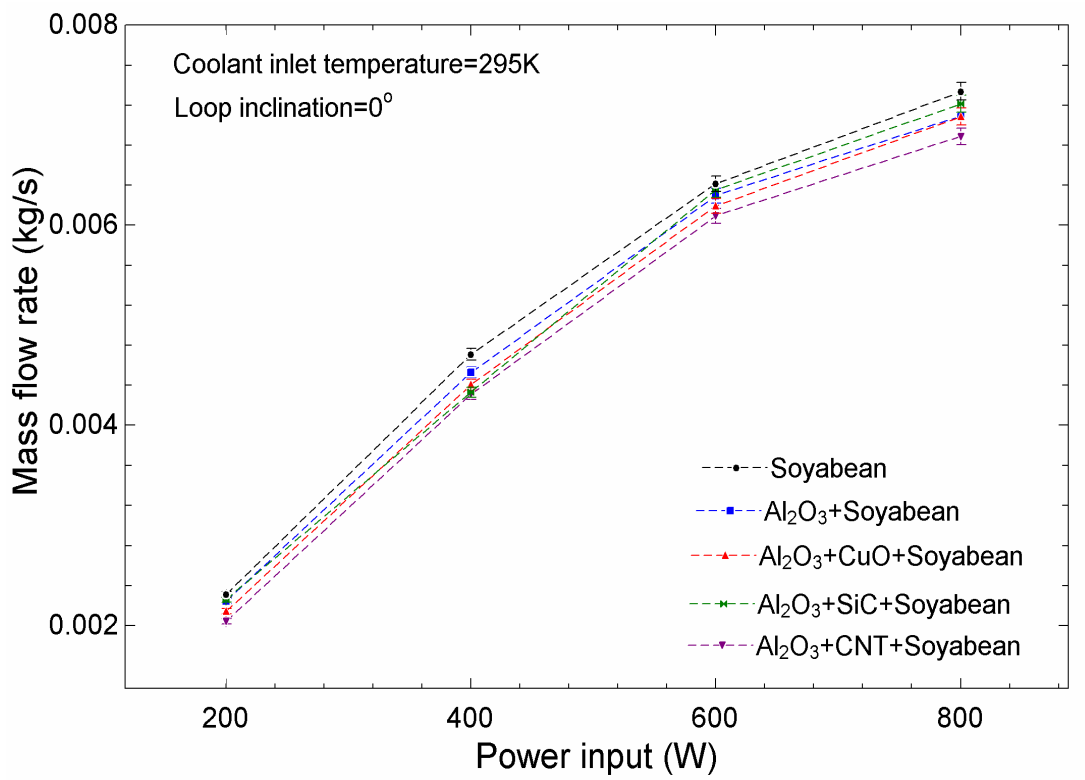

Fig. 6.11 Steady state mass flow rate for different soyabean-based mono/hybrid nanofluids with power input.

The steady-state effectiveness of the cooler for Therminol VP1 oil and Soyabean oil-based nano-oils at different input powers is shown in Fig. 6.12 and Fig. 6.13, respectively. The following can be inferred from these figures:

(a) The effectiveness decreases with the input power for all the working fluids. The mono and hybrid nano-oils show higher effectiveness compared to the corresponding base fluids.

(b) The hybrid nano-oils with Al_2O_3+CNT show the highest effectiveness among all nano-oils and base fluids.

(c) In general, TVP1-based nano-oil has a lower effectiveness compared to Soyabean-based nano-oils for the considered input power.

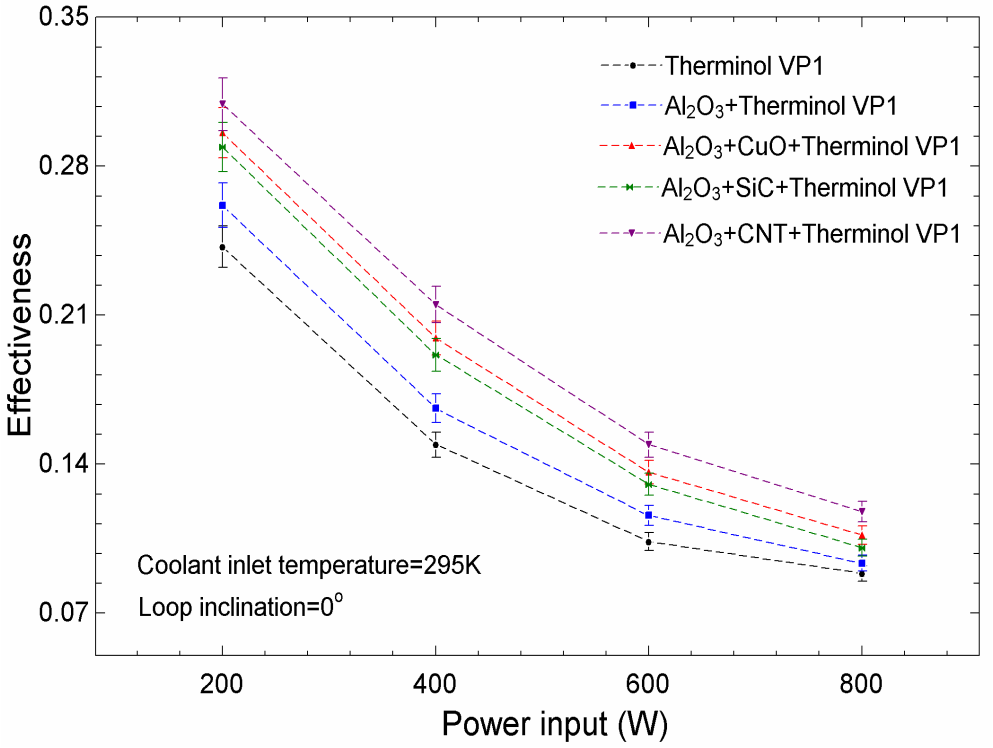

Fig. 6.12 Steady-state effectiveness of cooler for TVP1 based nano-oils for the different input powers

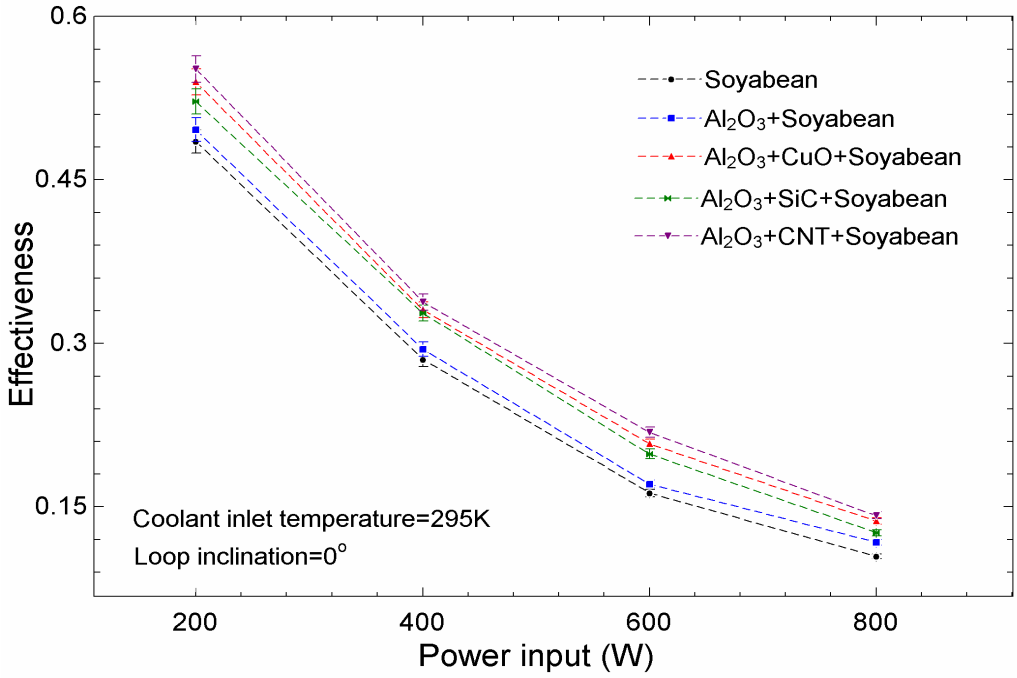

Fig. 6.13 Steady-state effectiveness of cooler for Soyabean oil and its nano-oils for the different input powers.

Fig. 6.14 and Fig. 6.15 demonstrate the effect of input power on the total entropy generation rate in the SPNCL for TVP1, Soyabean oil, and their nano-oils, respectively. It depicts that the entropy generation increases with increasing power input. This is attributed to the irreversibility arising out of the heat transfer rate and pressure drop. With the increasing input power, the heat transfer and pressure drop increase, and hence the entropy generation increases. For a given power, the entropy generation rate for base fluid is the highest for both the base fluids. Thus, an improvement in the exegetic performance of SPNCL using nanofluids is postulated. In particular, the nanoparticles, Al_2O_3+CNT, show the minimum total entropy generation rate compared to all the other combinations. The maximum reduction in the total entropy generation rate for Al_2O_3+CNT+TVP1 is about 19% and for Al_2O_3+CNT+Soyabean oil is about 13% at the highest input power 800 W compared to the respective base fluids.

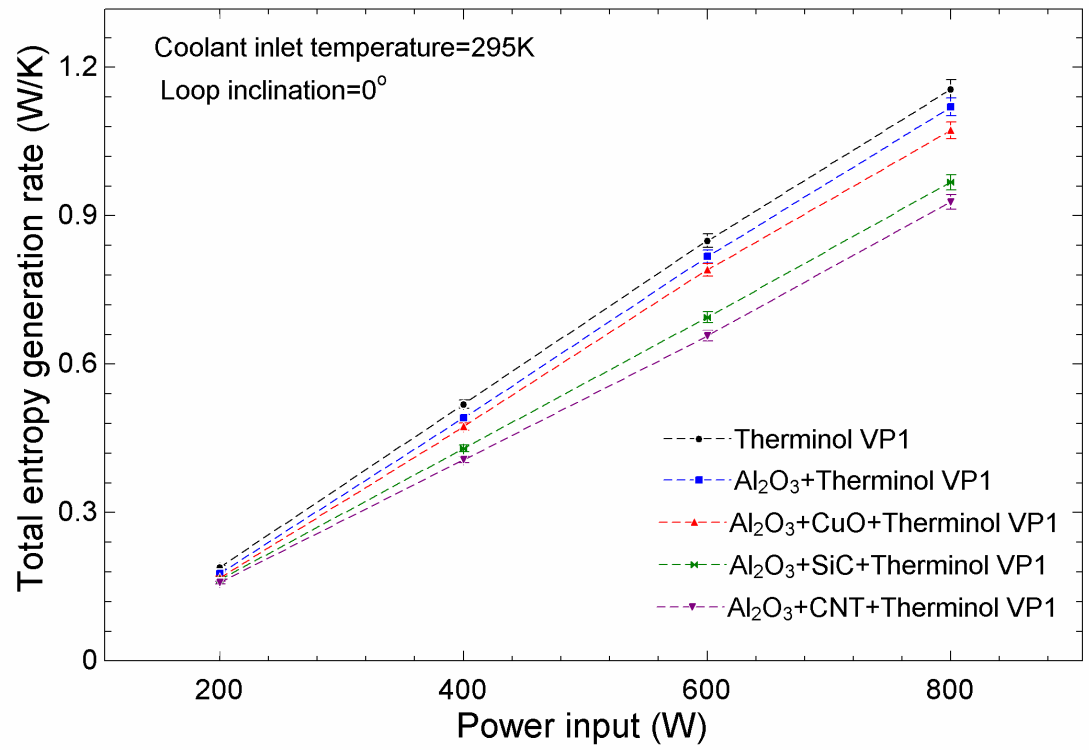

Fig. 6.14 The total entropy generation rates at the steady-state conditions for TVP1 and TVP1-based nano-oils at different input powers

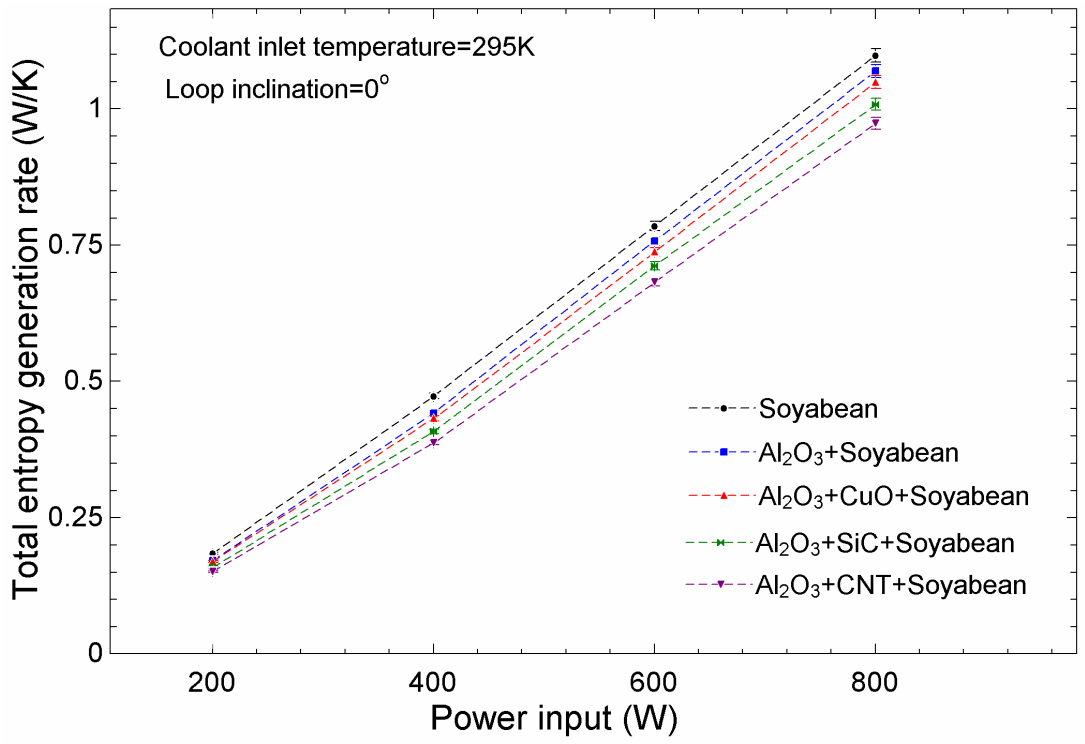

Fig. 6.15 The total entropy generation rates at the steady-state conditions for Soyabean oil and Soyabean oil-based nano-oils at different input powers.

6.2.5 Effect of loop inclination on the performance parameters

In this section, the effect of loop inclination (counter-clockwise and clockwise) on the performance parameters has been investigated, see Fig. 6.16 (a) and (b). There, the counter-clockwise inclination angle is designative with a negative sign, whereas the clockwise inclination angle is designated with a positive sign. It is worthwhile to note that the level differences between the center of gravity between the heater and cooler, will be different for the counter-clockwise and the clockwise inclinations. This is expected to influence the performance of SPNCL and is of practical and fundamental interest. Moreover, there is a dearth in literature exploring this aspect.

(a) (b)

Fig. 6.16 The photographs showing VHHC arrangement of SPNCL with (a) counter-clockwise and (b) clockwise inclinations

Fig. 6.17 and Fig. 6.18 show the time-dependent temperature difference across the heater for different angle of inclinations with TVP1 and Soyabean oil, respectively, at an input power 400 W. This figure depicts that the temperature difference is the minimum for the vertical (0^0) loop and maximum for the clockwise inclination of $+60^0$ for both the fluids. This is attributed to the reduction in effective height between the heater and cooler, which decreases the bouncy or the resulting mass flow rate and consequently the highest temperature difference. An analysis for the difference in center of gravity between the heater and cooler is presented in Fig. 6.19. This re-confirms the observation and allows recommendation that the clockwise inclination of SPNCL must be avoided during practical application.

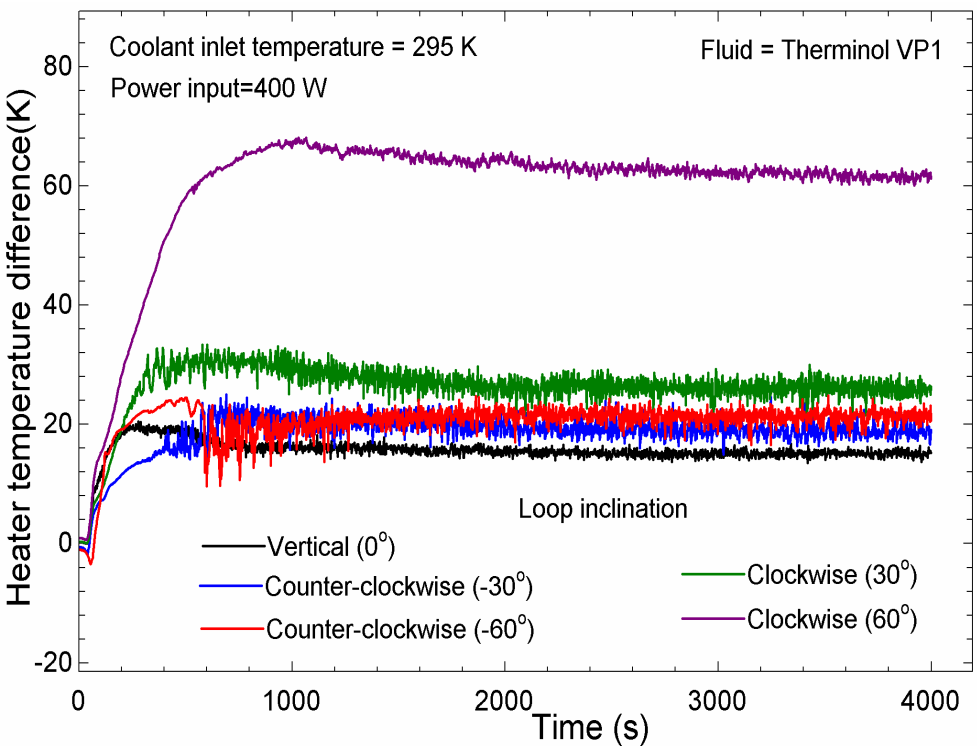

Fig. 6.17Experimental transient temperature differences across the heater for the different loop inclinations with TVP1

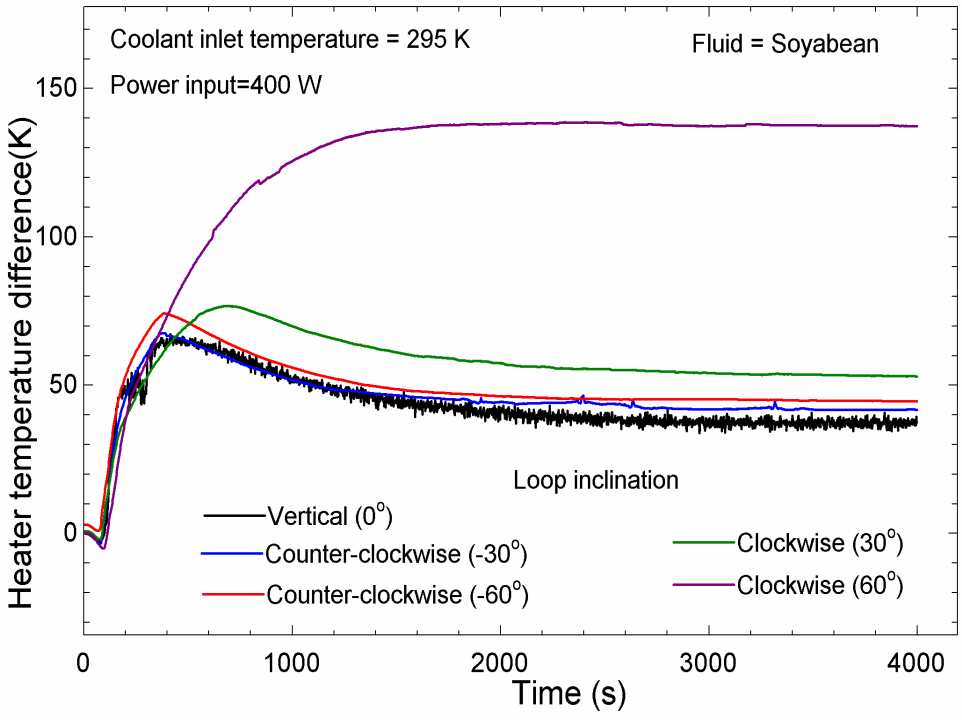

Fig. 6.18 Experimental transient temperature differences across the heater for the different loop inclinations with Soyabean oil

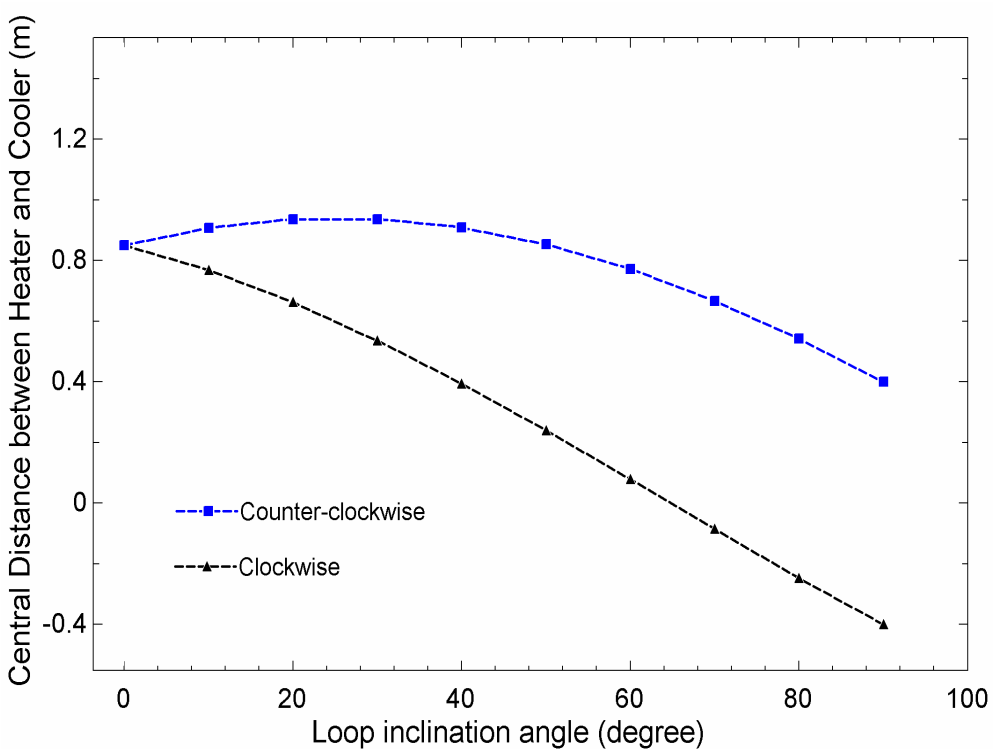

Fig. 6.19 Variation of the central distance between heater and heat exchanger at different loop inclinations

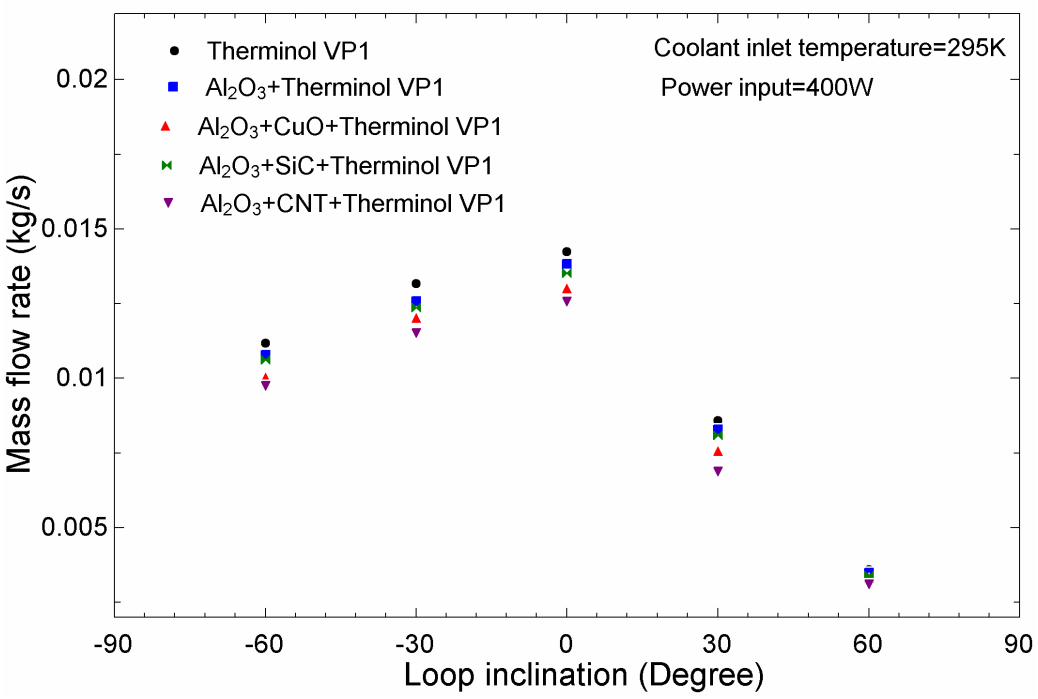

Fig. 6.20 Steady state experimental mass flow rate for different Therminol VP1-based mono/hybrid nanofluids at different loop inclinations

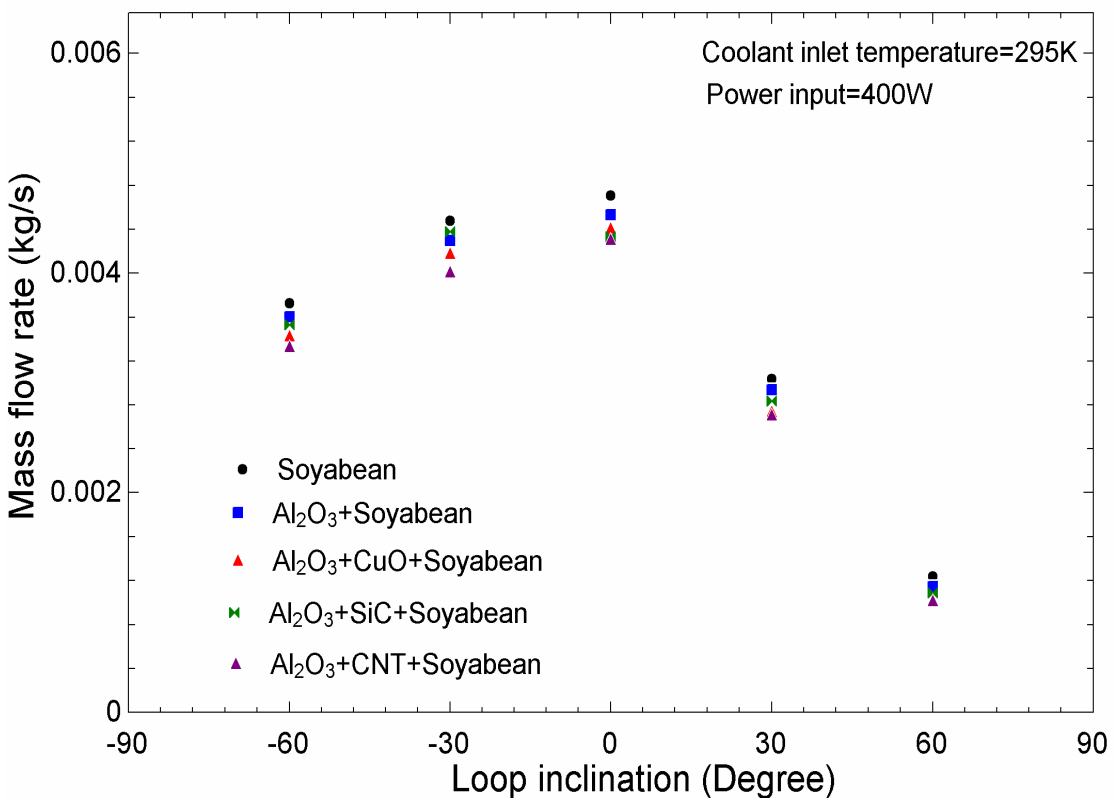

Fig. 6.21 Steady-state experimental mass flow rate for different Soyabean-based mono/hybrid nanofluids at different loop inclinations

Fig. 6.20 and Fig.6.21 show the steady-state mass flow rates, at different loop inclinations, for TVP1, Soyabean oil, and their nano-oils at an input power 400 W. As inferred in the previous discussion, the mass flow rate decreases with the increasing loop inclinations. However, the decrease for the clockwise inclination seems to be larger than that of the counter-clockwise inclination. This is attributed to the effective height between the heater and cooler, which is less for the clockwise inclination, see Fig.6.19. This reduces the buoyancy, which leads to a reduction in mass flow rate. The reduction in mass flow rate is ~7% and ~21% for experiments with the counter-clockwise inclination and ~39% and ~73% for clockwise inclination at 30^0 and 60^0, respectively, for TVP1 with respect to the vertical position (0^o).

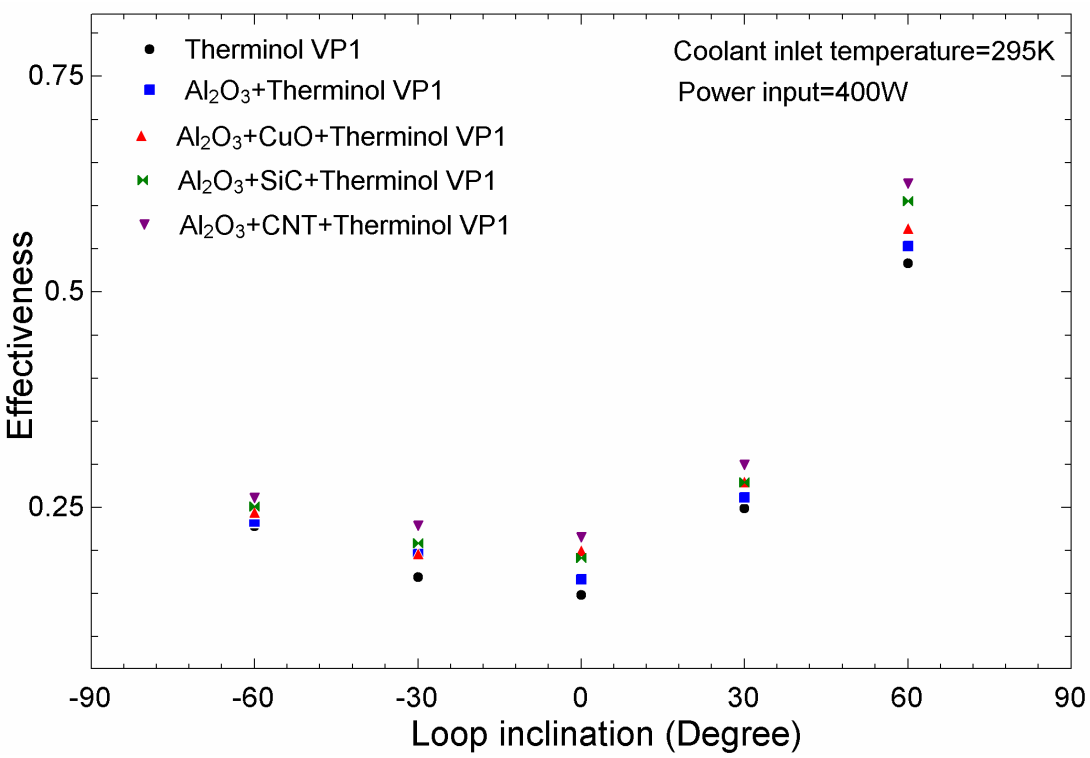

Fig. 6.22 Steady state experimental effectiveness for different Therminol VP1-based mono/hybrid nanofluids at different loop inclination

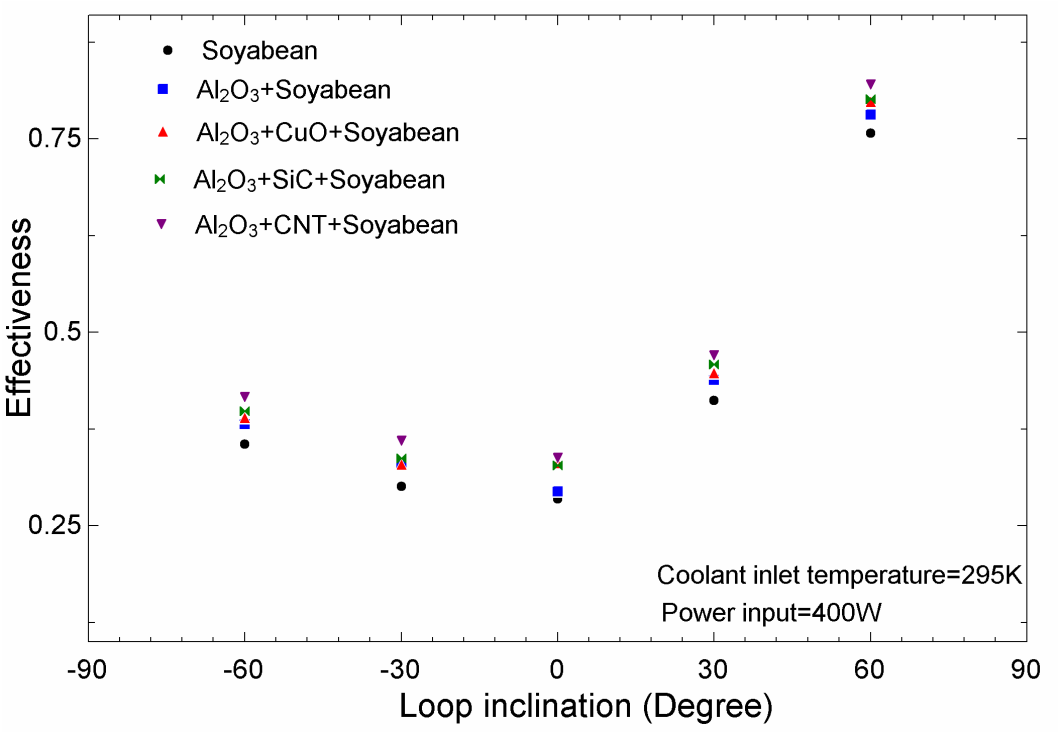

Fig. 6.23 Steady state experimental effectiveness for different Soyabean-based mono/hybrid nanofluids at different loop inclination

Fig. 6.22 and Fig. 6.23 demonstrate the effect of loop inclination on the effectiveness of heat exchanger for Therminol VP1 and Soyabean oil-based mono/hybrid nanofluids at 400 W, respectively. From the figures, it can be observed that the effectiveness of the heat exchanger increases with the loop inclination for all the working fluids. This is attributed to the decreasing mass flow rate with the increasing loop inclination. This leads to an increase in the temperature difference ($T_{C,in}$-T_{Cout}). The heat transfer coefficient decreases due to a decrease in mass flow rate, which increases the heat exchanger outlet temperature; hence the temperature difference ($T_{C,in}$-$T_{S,in}$) increases. Since both temperature differences ($T_{C,in}$-$T_{C,out}$) and ($T_{C,in}$-$T_{S,in}$) increase, so the overall effect will depend on which has a higher rate of increment. The rate of increment in the numerator is higher than the denominator; hence the effectiveness is increased.

Fig.6.24 and Fig.6.25 demonstrate the effect of loop inclination on the total entropy generation rate for Therminol VP1 and Soyabean oil-based mono/hybrid nanofluids at 400 W, respectively. It is observed that the total entropy generation increases with the increasing loop inclination on both sides compared to the vertical loop for all the working fluids. The possible reason is that the entropy generation depends on the irreversibility due to heat transfer and pressure drop. At a given power input, the total entropy generation mainly depends on the mass flow rate, heater wall temperature and temperature ratio (T_{out}/T_{in}) (see Eqs. 6.9 to 6.12). The mass flow rate decreases with increasing loop inclination, which increases the temperature difference between the hot leg and cold leg, hence increasing in TR value which increases the entropy generation. The wall temperature also increases with increasing loop inclination due to a decrease in heat transfer coefficient, which increases the entropy generation. Since both temperature ratio and heater wall temperature increase the entropy generation, and a decrease in mass flow rate reduces the

total entropy generation rate, hence the net change in the total entropy generation depends on the dominance of these factors.

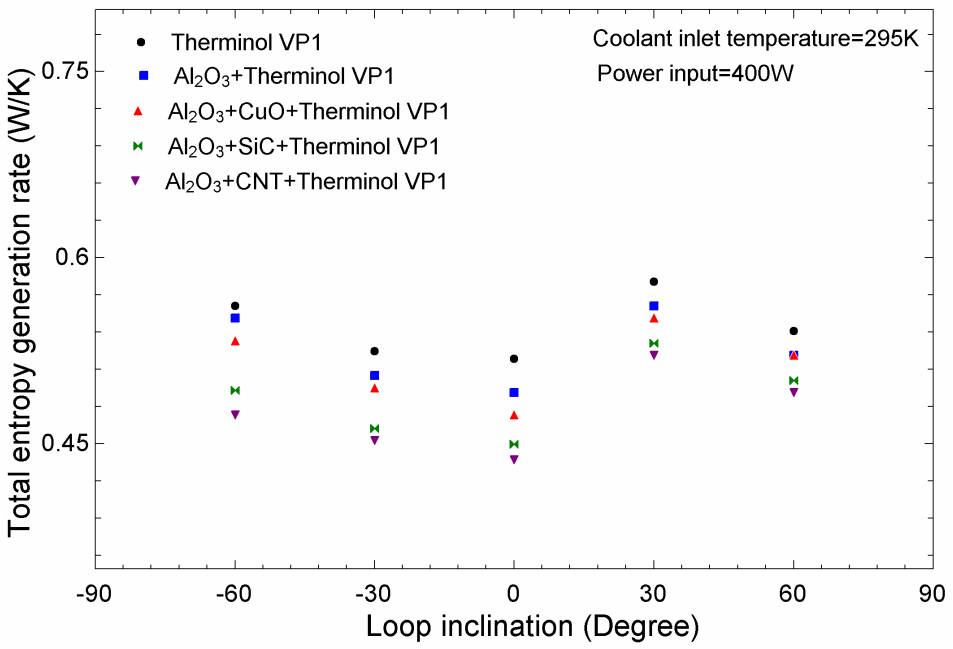

Fig. 6.24 Steady state experimental total entropy generation rate for different Therminol VP1-based mono/hybrid nanofluids at different loop inclination

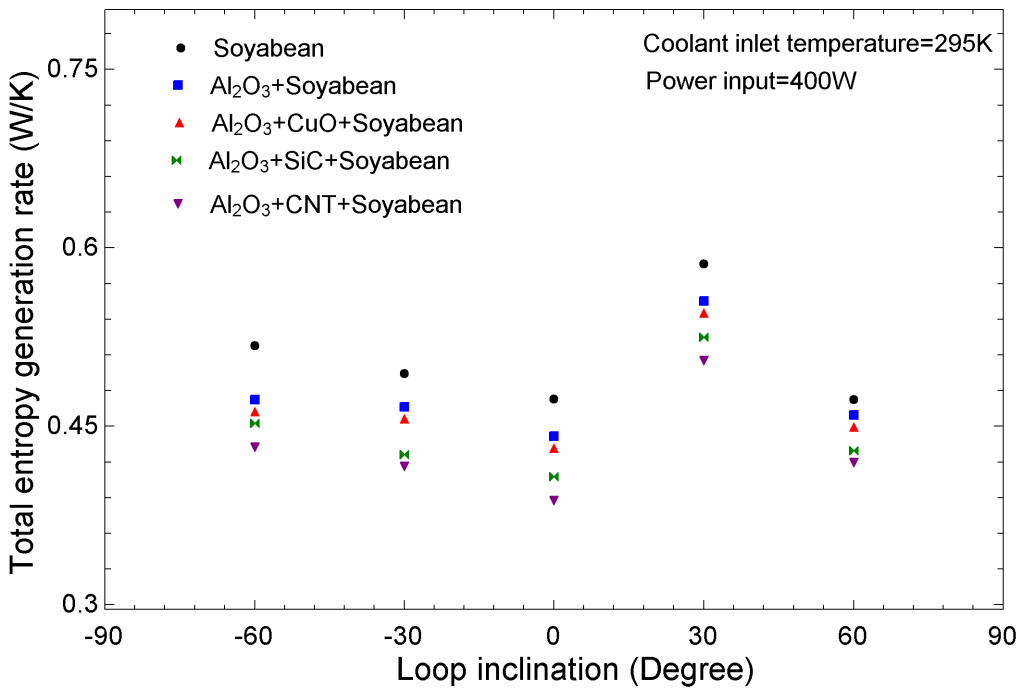

Fig. 6.25 Steady state experimental total entropy generation rate for different soyabean-based mono/hybrid nanofluids at different loop inclination

6.2.6 Performance comparison of Therminol VP1 and Soyabean oil

A comparative assessment of the performance of VHHC configuration of SPNCL with TVP1, Soyabean oil, and their hybrid-nano-oils with Al2O3+CNT is presented.

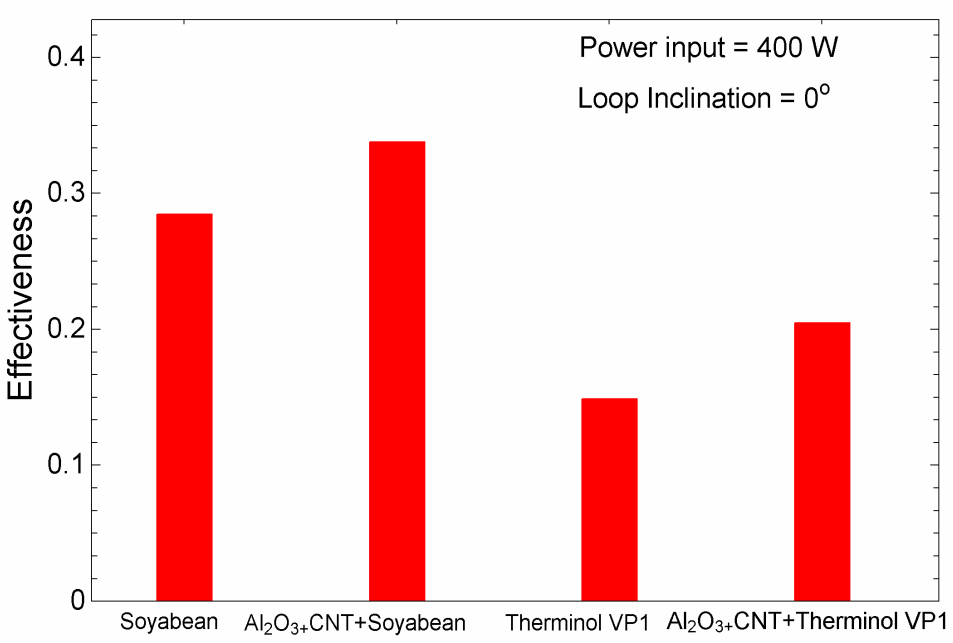

(a)

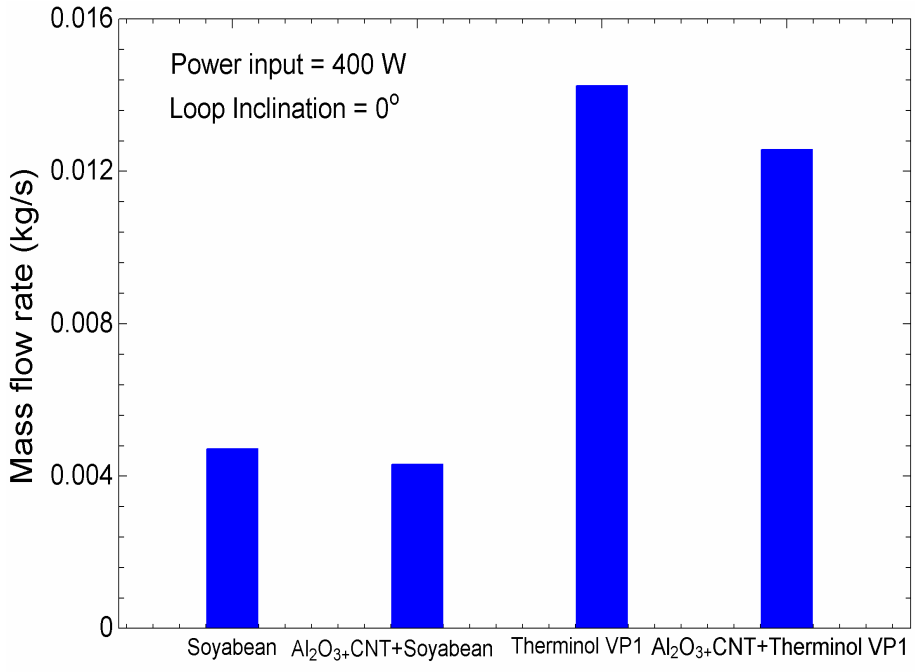

(b)

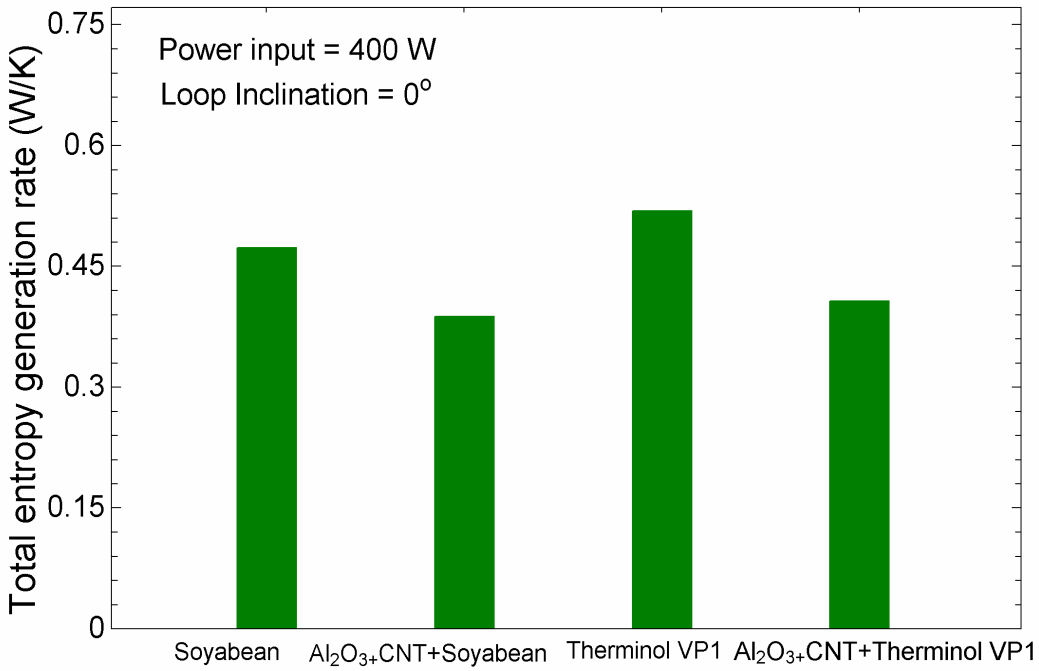

(c)

Fig. 6.26 Performance assessment of VHHC configuration of SPNCL with TVP1 with Soyabean oil based on (a) mass flow rate (b) effectiveness and (c) total entropy generation rate

Fig.6.26 shows that the mass flow rate is ~3 times higher for TVP1 compared to Soyabean oil, whereas the effectiveness is higher for soyabean oil. Moreover, the entropy generation rate is almost comparable. Since the mass flow rate defines the heat transport capability of any SPNCL system, which is a more desirable parameter compared to the effectiveness of the heat exchanger. Hence, TVP1 fluid may be preferred over Soyabean oil. Moreover, Al_2O_3+CNT nanofluid shows very less reduction in mass flow rate ~(7% to 9%), whereas it increases the effectiveness ~(25% to 30%) and decreases the total entropy generation rate ~(18% to 22%) compared to base fluids. Hence, the Al_2O_3+CNT can be preferred over base fluids for batter energetic and exergetic performance.

6.3 Important findings

- Spherical nanoparticle-based hybrid nanofluids yield a higher mass flow rate than cylindrical nanoparticle-based hybrid nanofluids.
- The Al_2O_3+MWCNT+Water hybrid nanofluids show higher effectiveness and the lowest total entropy generation rate compared to all the hybrid nanofluids.
- The Therminol VP1 oil shows better performance (mass flow rate, cooler effectiveness and entropy generation rate) than soyabean oil.
- The steady mass flow rate and total entropy generation rate increase and the effectiveness decreases with increasing power input.
- The loop inclination decreases the mass flow rate, whereas it increases the effectiveness and total entropy generation rate. The counter-clockwise inclination of the loop shows a lower reduction in mass flow rate compared to the clockwise inclination due to less reduction in the central distance between the heater and cooler.